Chapter 6

Hydrogenated and nitrogenated graphene for field effect gas sensing

This work reports the sensing responses of hydrogenated and nitrogenated graphene field effect transistors to various gas species including ethylene, carbon monoxide and ethanol. The two graphene devices are compared in terms of electrical properties and sensing performance corresponding to the surface functionalization. Superior to the responses of pristine graphene, hydrogenated graphene with more positive doping effect shows a higher sensitivity than nitrogenated graphene. The comparable responses to different gas on each device suggest a low selectivity of the functionalized graphene. Importantly, the real-time responses for hydrogenated graphene show a positive correlation with increased concentrations of ethylene. In contrast, the responses of nitrogenated graphene exhibit minimal or even decreased dependency to increased gas concentrations. Higher levels of nitrogen doping further decrease the sensitivity due to the doping transition from p-type to n-type. Therefore, chemical functionalization governs the sensitivity of graphene to a range of gas depending on changing the doping effect and adsorption affinity.

This chapter is prepared as an article: Lin Jiang, Wangyang Fu, Elisabeth Bouwman, Grégory F. Schneider, manuscript to be submitted

6.1 Introduction

Graphene, a single layer of sp^2 hybridized carbon atoms,[1] has been considered as an ideal sensing platform due to its large surface-to-volume ratio, being sensitive to surroundings and low electrical noises.[2] Especially, graphene field effect transistors (GFETs) utilizing the conductivity/resistivity responses can sensitively detect gas species down to single-molecules.[3] However, the absence of dangling bonds and the chemical inertness of the basal plane limit the detection sensitivity and selectivity of GFETs. As a result, the chemical modifications of the graphene surface have been extensively developed to improve the sensing performance of sensing devices.[4] For example, hydrogenation (Chapter 2) and nitrogenation (Chapter 3) have been conducted to not only introduce chemical defects and charge doping into the lattice, but also enhance the chemical and electrochemical reactivity of graphene.[5] In this chapter, we systematically investigated whether hydrogenation and nitrogenation by doping and defect generation could improve or modify the sensing performance of GFET devices.

Here, the field effect detection of ethylene, carbon monoxide and ethanol was explored at hydrogenated and nitrogenated graphene, referred as HG and NG. For that, hydrogen and ammonia plasmas were used to chemically functionalize the graphene. With a similar defect density, p-doped HG and NG showed improved responses to the tested gas compared to pristine graphene. The influence of the electron mobility and of charge doping on the sensing performance were investigated in details. A lower electron mobility was not found to limit the highest sensitivity of HG. Nitrogenation (exposure time longer than 10 s) formed n-doped NG with decreased sensitivity compared to the p-doped NG containing lower levels of nitrogenation. Surface ageing induced p-doping and enhanced sensitivity. In contrast to NG, the real-time responses of HG exhibited a positive correlation to the increasing concentration of ethylene. The responses to carbon monoxide and ethanol for both HG and NG showed no correlations to the measured concentrations.

6.2 Results

6.2.1 Raman characterization of graphene

Raman spectroscopy was performed to characterize the defect density and nature of chemical vapor deposition (CVD) graphene supported on a silicon wafer upon hydrogenation and nitrogenation treatments. The Raman spectra of pristine graphene in Figure 6.1a is characterized by two peaks, the G peak (1584 cm^{-1}) and the 2D peak (2681 cm^{-1}). In addition to the sharp and single-Lorentz fitted 2D peak, the intensity ratio $I(2D)/I(G)$ (~2) and no visible D peak (~1350 cm^{-1}) indicate the monolayer nature of graphene with a negligible intrinsic defect density. After a

hydrogen plasma treatment of 30 s to 60 s, a D peak and D' peak (~1620 cm^{-1}) appeared due to the activation of H-sp^3 defects.[6] Similarly, ammonia plasma treatments from 10 s to 60 s also introduced nitrogenated defects and thus D and D' defect peaks (Figure 6.1b).

The intensity ratio I(D)/I(G) is an indicator of the defect density in HG and NG.[7] Compared to hydrogenation, nitrogenation introduced more defects into the graphene lattice with a I(D)/I(G) ratio for NG larger than for HG (Figure 6.1c). Moreover, the ratios of I(D)/I(D') in Figure 6.1d also suggest different defect nature for hydrogenated (~10, sp^3 type) and nitrogenated (~6, vacancy-like type) graphene.[8] As 30 s hydrogenation and 10 s of nitrogenation give rise to the similar defect density in graphene, their electrical properties and sensing performance were compared.

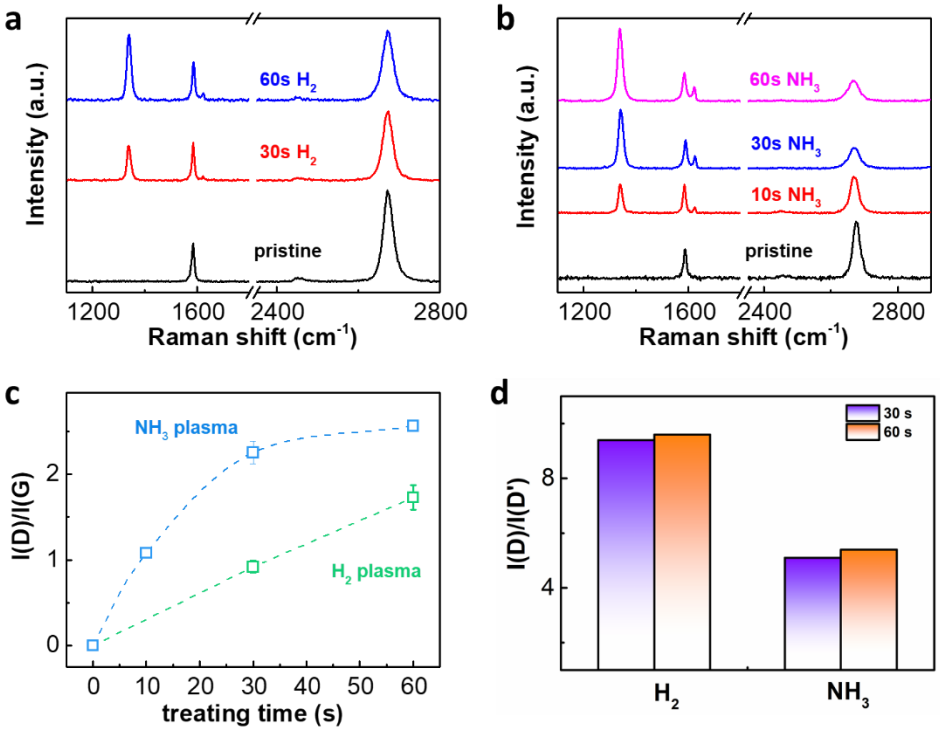

Figure 6.1 Raman characterization of HG and NG. a) Raman spectra of pristine graphene and graphene after 30 s and 60 s of hydrogen plasma treatment. b) Raman spectra of graphene after 0 s (pristine), 10 s, 30 s and 60 s of ammonia plasma. c) Intensity ratio I(D)/I(G) of graphene (a reflection of defect density) versus the treating times for HG and NG. d) I(D)/I(D') ratios of 30 s to 60 s of HG and NG.

6.2.2 The impact of electron mobility on the sensing performance

Graphene field effect transistor (GFET) devices were fabricated using polymer-assisted transfer. In details, chemical vapor deposition (CVD) graphene supported by the as-grown copper foil was spin-coated with a 400 nm thin layer of PMMA (poly(methyl methacrylate)).[9] After the copper was etched using an aqueous solution of ammonium persulfate (0.5 M), the graphene-PMMA assembly was then rinsed with ultra-pure water to remove any residues from the etchant. Finally a hydrophilic and clean silicon wafer (with a 285 nm-thick silicon dioxide layer on top) was used as a substrate of the graphene/PMMA assembly. Then the dried sample was immersed in acetone to remove PMMA and to expose the graphene surface. Source and drain electrodes (5 nm Cr/50 nm Au) were further deposited on top of graphene to ensure good and stable contacts with minimized contact resistance.

The resistance (R) of graphene was measured at gate voltages (V_g) in a back gated device configuration. The resistance-voltage (R-V_g) curves for 30 s HG and 10 s NG are plotted in Figure 6.2a. Owing to the p-doping effect from the trapped states at the substrate-graphene interface, pristine graphene intrinsically exhibits a positive charge neutrality point (CNP) of around 40 V. In contrast, positive CNP shifts compared to the pristine graphene were obtained for both HG (~110 V) and NG (~40 V). According to the discussion in Chapter 2 and 3, the p-doping effect for HG is mainly caused by the water adsorption[10] while for NG p-doping is primarily caused by the presence of pyridinic nitrogen dopants.[11] Subsequently, the mobility of different graphene samples were compared and plotted in Figure 6.2b. For pristine graphene, the hole carrier mobility is as high as ~1000 $cm^2 V^{-1} s^{-1}$, suggesting the high quality of the CVD graphene. In comparison, 10 s NG shows a slightly decreased mobility while 30s HG shows a much decreased mobility of ~500 $cm^2 V^{-1} s^{-1}$. As the carrier mobility of graphene is prone to charge scattering,[12] the reduced mobility of HG was mainly ascribed to the hybridization change and induced short-range scatterings in the lattice.[10, 13]

The sensing responses of graphene towards ethylene (0.1 ppm), carbon monoxide (0.01 ppm) and ethanol (1 ppm) were recorded in terms of the effective gate shifts, which are directly correlated to the graphene conductance using the transconductance.[3a] Superior to the responses on a pristine graphene, the 30 s HG shows larger shifts than 10 s NG, presumably because of a higher affinity of HG towards the adsorption of gas. Such a superiority of HG to NG is found to be coincident with the more positive p-doping effect as shown in Figure 6.1a. Separately, each type of GFET devices shows comparable responses between ethylene, carbon monoxide and ethanol within the tested concentrations, indicating a low selectivity to

any of the three gas. Therefore, hydrogenated and nitrogenated defects in graphene can enhance the sensitivity rather than the selectivity to gas detection. Separately, p-doping is favorable to the non-selective gas adsorption at the surface of graphene. More importantly, the mobility of graphene is not ruling the sensing sensitivity of graphene devices.

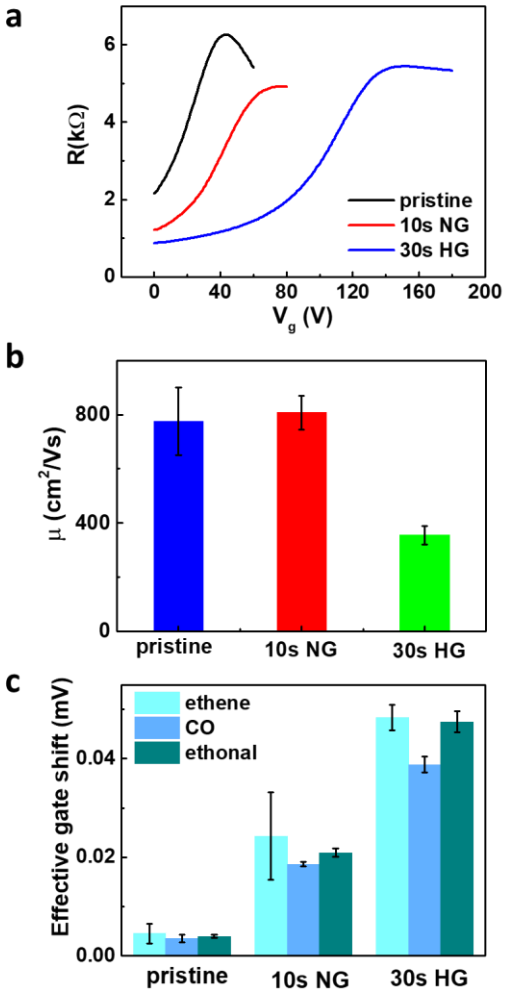

Figure 6.2 Comparison of transport properties and sensing performance for HG and NG. a) Resistance (R)-gate voltage (V_g) curves of pristine graphene, 30 s HG and 10 s NG. b) Comparison of graphene mobilities for pristine graphene, 30 s HG and 10 s NG. c) Effective gate shifts for pristine graphene, 30 s HG and 10 s NG following the exposure of the GFET devices to 0.1 ppm ethylene, 0.01 ppm carbon monoxide and to 1 ppm ethanol.

6.2.3 Real-time sensing responses

To further investigate the sensing performance, the resistance changes for 30 s HG and 10 s NG as a function of gas exposure time were compared (Figure 6.3). In Figure AV. 1, the graphene sheet resistance shows a time dependent drift of the baseline at the applied V_g of 0 V and constant exposure to technical air (free of water). After several seconds in presence of 0.1 ppm ethylene, sharp spikes appear due to the disturbance of the surface equilibrium following the introduction of gas molecules. Upon continuous exposure to ethylene, the resistance shows a staircase-like drop, which is caused by the adsorption of ethylene and the induced charge transfer to graphene.[14] The newly formed baseline indicates that the gas adsorption reaches an equilibrium. Finally flushing technical air leads to the desorption of ethylene from the graphene surface with the resistance of the device returning to its original equilibrium and baseline.

Figure 6.3a-c shows the resistance responses of the GFETs devices to the increasing concentrations of ethylene (0.1, 0.2, 0.5 ppm), carbon monoxide (0.01, 0.02, 0.05 ppm) and ethanol (1, 2, 5, 10 ppm) in sequence. The detection to each concentration is duplicate. The average responses of HG and NG are summarized in Figure 6.4d. In general, HG shows more sensitive responses than NG to the measured concentrations of all the three gas, which is consistent with the results obtained in Figure 6.2c. For detection of ethylene within the range of measured concentrations, the responses at 30 s HG shows an monotonic increasing dependency. For continuous detection of carbon monoxide, HG starts to show saturated responses when the concentration increases from 0.02 ppm to 0.05 ppm. After the saturation, the responses even decrease upon increasing concentrations of ethanol. In comparison, NG shows saturated responses to ethylene detection at concentrations from 0.1 to 0.2 ppm, followed by a decreasing trend of responses to increased concentrations of carbon monoxide and ethanol detection. The saturation trend after several times of detection can be attributed to that the limited active sites on the graphene surface are occupied by the trapped gas molecules. More detections induce more trapping and thus further reduce the available sites for valid gas adsorption to generate corresponding responses. As a consequence, NG is expected to have less active sites and thus be more prone to give saturated responses than HG.

Furthermore, the adsorption transient behaviors of the GFETs upon the exposure of different concentrations of ethylene gas molecules is summarized in Table 1. The adsorption transient parameter is defined as the resistance change ΔR vs the time required for the signal to reach the new baseline Δt, $\Delta(\Delta R/\Delta t)$. It is shown that upon the increase of ethylene concentrations, the transient parameter increases while

adsorption time decreases for both GFETs. Given the similar adsorption times between two types of GFETs, the higher values of adsorption transient parameters on HG than NG also reflect the more excellent sensing responses of HG in comparison with NG.

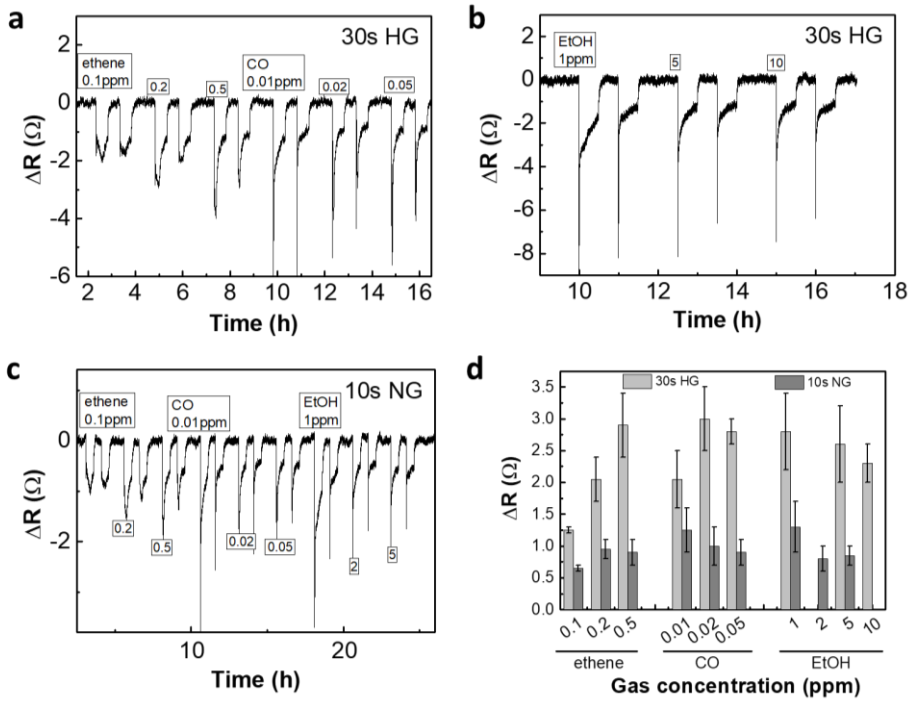

Figure 6.3 Real-time responses for HG and NG. a) Responses of 30 HG to ethylene (0.1, 0.2, 0.5 ppm) and CO (0.01, 0.02, 0.05 ppm). b) Responses of 30 s HG to EtOH (1, 5, 10 ppm). Each gas injection repeated once. c) Responses of 10 s NG to the exposure of ethylene (0.1, 0.2, 0.5 ppm), CO (0.01, 0.02, 0.05 ppm) and EtOH (1, 2, 5 ppm). Each gas injection was duplicated. d) Average resistivity responses for 30 s of HG and 10 s of NG for different gas. All the measurements were done at room temperature.

Table 1 Adsorption transient parameter and adsorption time for different concentrations of ethylene on GFETs

GFETs	Gas concentration (ppm)	$\Delta(\Delta R/\Delta t)$ (ohm/sec)	Adsorption time Δt (sec)
30s HG	0.1	0.035	54
	0.2	0.076	32.4
	0.5	0.193	16.2
10s NG	0.1	0.016	46.8
	0.2	0.026	36
	0.5	0.063	18

6.2.4 The charge doping effect on the sensing performance

To gain insights into the effect of electrical doping on the GFETs sensing performance, graphene with different levels of surface freshness and nitrogenation were further studied. As illustrated in Figure 6.4a, the mobility generally decreases for graphene after ageing (~600 $cm^2 V^{-1} s^{-1}$) compared to the pristine graphene (~1000 $cm^2 V^{-1} s^{-1}$). Such a difference presumably originates from the presence of hydrocarbons adsorbed at the surface of graphene, acting as scatterers for charge carriers.[15] Correspondingly, aged graphene shows a p-doping behavior with a more positive CNP compared to pristine graphene (Figure 6.4b), which can be ascribed to the electron transfer from graphene to oxygen molecules dissolved in the adsorbed water layer at the surface of aged graphene.[16] As a result, the p-doping effect induced by ageing is likely to be responsible for the improved response of graphene (aged, without chemical functionalization) to 0.1 ppm ethylene (Figure 6.4c). This is also consistent with the observation that graphene with more p-doping shows a higher sensitivity in Figure 6.2.

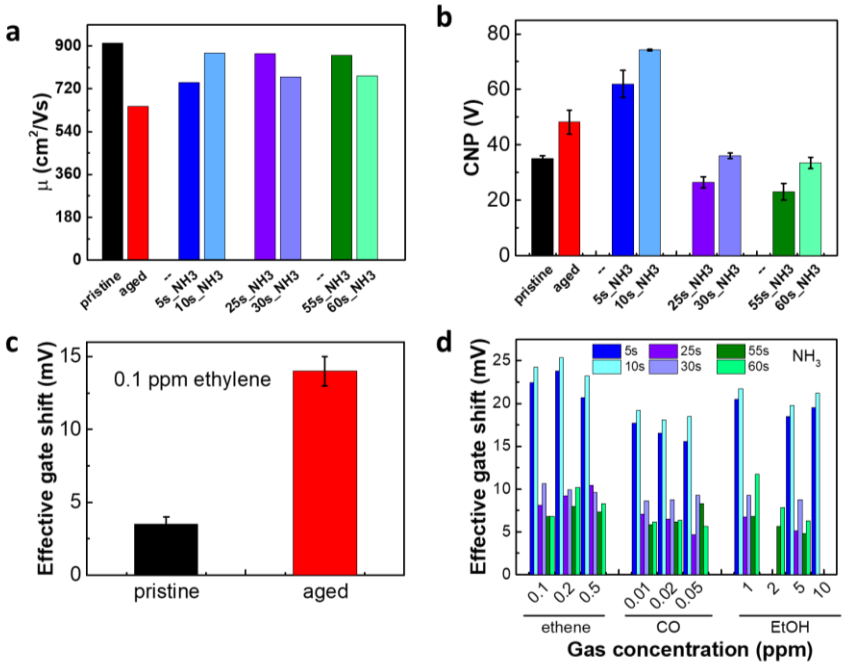

Figure 6.4 The charge doping effect on the GFETs sensing performance. a) The mobility for pristine, aged, nitrogenated graphene (5, 10, 25, 30, 55, and 60 s). b) The charge neutrality points (CNPs) of the graphene samples in a). c) The effective gate shifts for pristine and aged graphene to 0.1 ppm ethylene. d) Effective gate shifts for nitrogenated graphene (5, 10, 25, 30, 55, and 60 s) towards the detection of 0.1, 0.2, 0.5 ppm of ethylene, 0.01, 0.02, 0.05 ppm of CO and 1, 2, 5, 10 ppm of EtOH.

Figure 6.4a shows that nitrogenation only slightly decreased the mobility of graphene even when the treating time increased from 5 to 60 s. Compared to the CNP of pristine graphene (35 V), low levels of nitrogenation positively shift the CNP to 62 V (5 s) and 74 V (10 s) and induce a p-doping effect in graphene (Figure 6.4b). In contrast, further nitrogenation (25 to 60 s) negatively shifts the CNP to ~30V, forming n-doped NG as compared to the p-doped NG (5 to 10 s). According to the literature, pyridinic nitrogen causes p-doping while pyrrolic and graphitic nitrogen introduce n-doping effect in graphene.[11] Therefore, low levels of nitrogenation (5 to 10 s) are expected to mainly form pyridinic nitrogen dopants while pyrrolic and graphitic nitrogen dominate for higher levels of nitrogenation (25 to 60 s).

Figure 6.4d shows the effective gate shifts of different nitrogenated GFETs to the three gas species with increasing concentrations. It is found that more than 10 s of nitrogenation in graphene reduces the responses to all the gas species compared to those after 5 and 10 s. This trend coincides well with the doping transition from p-type to n-type in NG, further confirming that more p-doping in graphene favors the gas adsorption and thus more sensitive responses. Moreover, the responses on all the NG samples exhibit no dependency (or even decreased dependency) on the increasing gas concentrations. Such saturation effects in the sensing performance may be ascribed to the much higher adsorption coefficient than the desorption coefficient of the gas molecules from NG. As a consequence, NG is not a suitable sensing element for gas sensors regardless of the nitrogen doping levels.

6.3 Conclusions

Field effect transistors based on hydrogenated and nitrogenated graphene (HG and NG) have been successfully fabricated for the gas sensing of ethylene, carbon monoxide and ethanol. Compared to the pristine graphene, 30 s HG and 10 s NG both show enhanced sensitivity, however with low selectivity to each of the gas. A higher sensitivity is obtained on the HG with a higher p-doping effect, indicating that positive doping in graphene is related to the improved sensitivity. Besides, only the HG shows positively correlated real-time responses to increased ethylene concentrations. Meanwhile, higher levels of nitrogenation (25 to 60 s) in graphene decreases the responses compared to the low levels of nitrogenation (5 to 10 s). More importantly, p-doping induced by hydrogenation, low levels of nitrogenation and ageing are found to correlate with an increased sensitivity. In conclusion, chemical modification of graphene contributes to change the sensing sensitivity of several gas by introducing p or n doping by modifying the adsorption-desorption process. However, the influence of the surface modification on the selectivity is very limited. To improve the

selectivity via specific recognition between the surface functionalities of graphene and the analytes will have to be developed.

6.5 References

[1] K. S. Novoselov, A. K. Geim, S. V. Morozov, D. Jiang, Y. Zhang, S. V. Dubonos, I. V. Grigorieva, A. A. Firsov, *science* **2004**, 306, 666.

[2] a) K. S. Novoselov, A. K. Geim, S. Morozov, D. Jiang, M. Katsnelson, I. Grigorieva, S. Dubonos, Firsov, AA, *Nature* **2005**, 438, 197; b) C. Lee, X. Wei, J. W. Kysar, J. Hone, *science* **2008**, 321, 385.

[3] a) W. Fu, T. F. van Dijkman, L. M. Lima, F. Jiang, G. g. F. Schneider, E. Bouwman, *Nano Lett.* **2017**, 17, 7980; b) W. Fu, L. Jiang, E. P. van Geest, L. M. Lima, G. F. Schneider, *Adv. Mater.* **2017**, 29, 1603610.

[4] a) D. C. Elias, R. R. Nair, T. Mohiuddin, S. Morozov, P. Blake, M. Halsall, A. C. Ferrari, D. Boukhvalov, M. Katsnelson, A. Geim, *Science* **2009**, 323, 610; b) H. Feng, R. Cheng, X. Zhao, X. Duan, J. Li, *Nature communications* **2013**, 4, 1539; c) W. Fu, C. Nef, A. Tarasov, M. Wipf, R. Stoop, O. Knopfmacher, M. Weiss, M. Calame, C. Schönenberger, *Nanoscale* **2013**, 5, 12104; d) N. Dontschuk, A. Stacey, A. Tadich, K. J. Rietwyk, A. Schenk, M. T. Edmonds, O. Shimoni, C. I. Pakes, S. Prawer, J. Cervenka, *Nature communications* **2015**, 6, 6563; e) M. B. Lerner, F. Matsunaga, G. H. Han, S. J. Hong, J. Xi, A. Crook, J. M. Perez-Aguilar, Y. W. Park, J. G. Saven, R. Liu, *Nano Lett.* **2014**, 14, 2709.

[5] J. Duan, S. Chen, M. Jaroniec, S. Z. Qiao, *ACS Catal.* **2015**, 5, 5207.

[6] a) F. Tuinstra, J. L. Koenig, *J. Chem. Phys.* **1970**, 53, 1126; b) P. Lespade, A. Marchand, M. Couzi, F. Cruege, *Carbon* **1984**, 22, 375.

[7] L. G. Cançado, A. Jorio, E. H. M. Ferreira, F. Stavale, C. A. Achete, R. B. Capaz, M. V. O. Moutinho, A. Lombardo, T. S. Kulmala, A. C. Ferrari, *Nano Lett.* **2011**, 11, 3190.

[8] A. Eckmann, A. Felten, A. Mishchenko, L. Britnell, R. Krupke, K. S. Novoselov, C. Casiraghi, *Nano Letters* **2012**, 12, 3925.

[9] X. Li, Y. Zhu, W. Cai, M. Borysiak, B. Han, D. Chen, R. D. Piner, L. Colombo, R. S. Ruoff, *Nano Lett.* **2009**, 9, 4359.

[10] L. Jiang, W. Fu, Y. Y. Birdja, M. T. Koper, G. F. Schneider, *Nat. Commun.* **2018**, 9, 793.

[11] T. Schiros, D. Nordlund, L. Pálová, D. Prezzi, L. Zhao, K. S. Kim, U. Wurstbauer, C. Gutiérrez, D. Delongchamp, C. Jaye, *Nano Lett.* **2012**, 12, 4025.

[12] S. D. Sarma, S. Adam, E. Hwang, E. Rossi, *Rev. Mod. Phys.* **2011**, 83, 407.

[13] J. Balakrishnan, G. K. W. Koon, M. Jaiswal, A. C. Neto, B. Özyilmaz, *Nat. Phys.* **2013**, 9, 284.

[14] J.-H. Chen, C. Jang, S. Adam, M. Fuhrer, E. Williams, M. Ishigami, *Nat. Phys.* **2008**, 4, 377.

[15] Z. Li, Y. Wang, A. Kozbial, G. Shenoy, F. Zhou, R. McGinley, P. Ireland, B. Morganstein, A. Kunkel, S. P. Surwade, *Nat. Mater.* **2013**, 12, 925.

[16] Z. Peng, R. Yang, M. A. Kim, L. Li, H. Liu, *RSC Adv.* **2017**, 7, 27048.